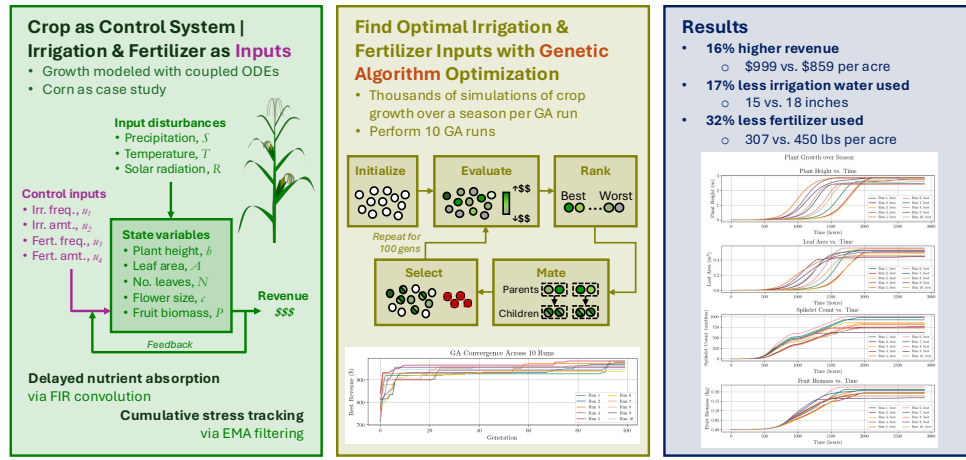


1 Graphical Abstract

2 Optimizing irrigation and fertilizer strategy using a crop growth model with delayed nutrient absorption dynamics

4 Carla J. Becker, Tarek I. Zohdi

Optimizing Irrigation & Fertilizer Strategy via Crop Model + Genetic Algorithm



UC Berkeley Carla J. Becker, Tarek I. Zohdi (2026)

5 Highlights

6 **Optimizing irrigation and fertilizer strategy using a crop growth**
7 **model with delayed nutrient absorption dynamics**

8 Carla J. Becker, Tarek I. Zohdi

- 9 • Reduced-order coupled ODE model; efficient alternative to DSSAT/AP-
10 SIM
- 11 • FIR convolution formulation for delayed nutrient absorption dynamics
- 12 • EMA filtering for cumulative environmental stress tracking
- 13 • GA optimization of irrigation/fertilization schedules to maximize rev-
14 enue
- 15 • Calibration and validation against Iowa corn agronomic data

¹⁶ Optimizing irrigation and fertilizer strategy using a crop
¹⁷ growth model with delayed nutrient absorption
¹⁸ dynamics

¹⁹ Carla J. Becker, Tarek I. Zohdi

^a*Department of Mechanical Engineering, University of California, Berkeley, 6141
Etcheverry Hall, Berkeley, 94720, California, United States of America*

^b*Department of Mechanical Engineering, University of California, Berkeley, 6141
Etcheverry Hall, Berkeley, 94720, California, United States of America*

²⁰ **Abstract**

Rising production costs and declining commodity prices have motivated farmers to seek computational tools for optimizing resource application. This paper presents a generalized, coupled ordinary differential equation (ODE) model for crop growth that captures the nonlinear dynamics of plant development under varying environmental conditions and fertilizer and irrigation strategy. The model tracks five state variables—plant height, leaf area, number of leaves, flower size, and fruit biomass—each governed by logistic growth with time-varying growth rates and carrying capacities. These parameters are modulated by nutrient factors that quantify how well actual water, fertilizer, temperature, and solar radiation levels match expected values. To capture the delayed physiological response of plants to resource inputs, we employ finite impulse response (FIR) convolution with Gaussian kernels, where different temporal spreads represent the distinct metabolic timescales for each input type. Cumulative divergence from expected nutrient levels is tracked using exponential moving average filters, providing the model with memory of past stress events. Given this nonlinear, delay-affected system, we employ a genetic algorithm (GA) to discover optimal irrigation and fertilizer strategies that maximize crop yield while minimizing input costs. The GA searches over application frequency and amount for both irrigation and fertilizer, evaluating candidate strategies through full-season simulations. We demonstrate the framework using corn grown in Fairfax, Iowa, with historical weather data. Results show the GA identifies non-intuitive strategies that outperform conventional uniform application schedules, achieving 16%

higher net revenue through strategic timing of resource inputs. The optimized strategies use dramatically less irrigation than farmer best practices while achieving higher crop yields, demonstrating that under delayed absorption dynamics, timing of inputs matters more than total quantity.

- 21 *Keywords:* precision agriculture, resource optimization, crop growth
22 model, genetic algorithm, cumulative stress tracking
-

23 **1. Introduction**

24 The agriculture sector in the United States faces significant challenges as
25 the number of farms declines and the cost of farming continues to rise [?].
26 Rising production expenses for equipment, seeds, and labor, coupled with
27 elevated interest rates and declining commodity prices, have made farming
28 increasingly expensive. To navigate this challenging landscape, farmers are
29 employing strategies such as cost management and operational optimization.
30 One promising approach is to use modeling and simulation to optimize farm
31 operations without substantial capital investment. Recent advances in com-
32 putational methods have enabled sophisticated digital-twin frameworks for
33 precision agriculture [? ?], and machine learning techniques have been
34 applied to optimize sensor placement and resource delivery in agricultural
35 systems [? ?].

36 Mathematical modeling of crop growth has a rich history, with models
37 ranging from simple empirical relationships to complex mechanistic simula-
38 tions. Logistic growth models, first proposed by Verhulst in 1838, remain
39 widely used due to their interpretability and ability to capture resource-
40 limited growth dynamics [?]. More sophisticated crop models such as
41 DSSAT [?], APSIM [?], and WOFOST [?] simulate detailed physio-
42 logical processes but require extensive parameterization and may be computa-
43 tionally expensive for optimization applications. In contrast, reduced-order
44 models that capture essential dynamics while remaining tractable for opti-
45 mization have gained attention in precision agriculture [?].

46 Optimization of irrigation and fertilizer application has been studied us-
47 ing various approaches, including linear and nonlinear programming [?],
48 dynamic programming [?], and metaheuristic algorithms [?]. Genetic algo-
49 rithms (GAs) are particularly well-suited for this domain because they can
50 handle nonlinear, non-convex objective functions and do not require gradi-
51 ent information [?]. Previous work has applied GAs to irrigation scheduling

52 [?] and fertilizer optimization [?], but these studies often use simplified
53 plant response models that do not capture the delayed, cumulative effects of
54 resource application.

55 This paper presents a generalized, coupled ordinary differential equation
56 (ODE) model for crop growth that addresses these limitations. The model
57 captures: (1) nonlinear logistic growth with state-dependent carrying ca-
58 pacities, (2) delayed absorption of water, fertilizer, temperature, and solar
59 radiation inputs through finite impulse response (FIR) convolution, (3) cu-
60 mulative stress tracking via exponential moving average (EMA) filters, and
61 (4) coupling between vegetative and reproductive growth stages. The model
62 is designed to enable global optimization under delayed, resource-coupled
63 dynamics—a regime where even well-established management practices may
64 benefit from computational refinement due to the sheer number of possible
65 scheduling combinations.

66 We demonstrate the framework by optimizing irrigation and fertilizer
67 strategies for corn, the most widely planted crop in the United States by
68 acreage. Using a genetic algorithm, we search for strategies that maximize
69 net revenue (crop value minus input costs) over a growing season. The ap-
70 proach is validated using historical weather data from Fairfax, Iowa, a rep-
71 resentative location in the Corn Belt.

72 2. Generalized, coupled-ODE crop model

73 The proposed model tracks five state variables representing key aspects
74 of plant development: plant height h (m), leaf area per leaf A (m^2), num-
75 ber of leaves N , flower size c (number of spikelets), and fruit biomass P
76 (kg). Each state variable follows logistic growth dynamics with time-varying
77 growth rates and carrying capacities that depend on environmental condi-
78 tions and resource availability.

79 The model receives four input signals: water from irrigation w (inches),
80 fertilizer application f (lbs), ambient temperature T ($^\circ\text{C}$), and solar radiation
81 R (W/m^2). Precipitation S (inches) is added to irrigation to obtain total
82 water input. Temperature and radiation data are obtained from the National
83 Solar Radiation Database (NSRDB) [?], while precipitation data comes from
84 NOAA historical records [?].

85 2.1. Delayed absorption via FIR convolution

86 Plants do not immediately process applied nutrients; instead, there is
87 a physiologically-mediated delay between application and utilization. We
88 model this delayed absorption using finite impulse response (FIR) convolu-
89 tion with Gaussian kernels.

90 If cumulative nutrient uptake follows a sigmoid trajectory—with slow ini-
91 tial uptake due to transport lag, rapid increase once metabolic pathways acti-
92 vate, and eventual saturation—then instantaneous absorption rate follows a
93 bell-shaped curve. A Gaussian kernel is the least assumptive choice for a bell
94 curve, requiring only two parameters: the temporal spread σ (characterizing
95 absorption duration) and the peak delay μ .

96 Given only the temporal spread σ for each nutrient type, we determine μ
97 such that 95% of the kernel mass lies within $[0, 2\mu]$. This requires solving

$$\operatorname{erf}\left(\frac{\mu}{\sigma\sqrt{2}}\right) = 0.95, \quad (1)$$

98 which yields $\mu \approx 1.96\sigma$. The Gaussian FIR kernel is then

$$g[k] = \frac{1}{\sqrt{2\pi\sigma^2}} \exp\left\{-\frac{1}{2} \frac{(k - \mu)^2}{\sigma^2}\right\}. \quad (2)$$

99 The FIR horizon L^* is chosen as the minimum length capturing 95% of
100 the kernel mass:

$$L^* = \min_L \left\{ L : \frac{\sum_{k=0}^{L-1} g[k]}{\sum_{k=0}^{K-1} g[k]} \geq 0.95 \right\} \quad (3)$$

101 where K is the simulation length in hours.

102 Different nutrients have different metabolic timescales. We use $\sigma_w = 30$
103 hours for water (rapid uptake), $\sigma_f = 300$ hours for fertilizer (slow uptake re-
104 flecting root absorption dynamics), and $\sigma_T = \sigma_R = 30$ hours for temperature
105 and radiation (immediate physiological effects with short memory).

106 2.2. Cumulative stress tracking via EMA filtering

107 While FIR convolution captures delayed absorption, plants also accumu-
108 late stress from sustained deviations from optimal conditions. We model this
109 cumulative effect using exponential moving average (EMA) filters, which are
110 equivalent to first-order infinite impulse response (IIR) systems.

111 The EMA filter with memory parameter $\beta \in [0, 1)$ has the recursive form:

$$y[k] = (1 - \beta)x[k] + \beta y[k - 1] \quad (4)$$

112 where larger β values correspond to longer memory (slower response to
113 changes). This formulation preserves constant signals ($x[k] = c$ implies
114 $y[k] \rightarrow c$) while smoothing transient fluctuations.

115 *2.3. Nutrient factor calculation*

116 We now describe the complete transformation pipeline that converts raw
117 input signals into nutrient factors $\nu \in [0, 1]$ that modulate plant growth. Us-
118 ing fertilizer as an example (the same process applies to water, temperature,
119 and radiation):

120 **Step 1: Delayed absorption.** Convolve the raw fertilizer signal $f[k]$
121 with the Gaussian FIR kernel:

$$\bar{f}[k] = \sum_{n=0}^{L_f-1} g_f[n] f[k-n] \quad (5)$$

122 **Step 2: Cumulative absorption.** Compute the running sum of ab-
123 sorbed fertilizer:

$$F[k] = \sum_{n=0}^k \bar{f}[n] \quad (6)$$

124 **Step 3: Instantaneous anomaly.** Compare actual cumulative absorp-
125 tion to expected levels:

$$\delta_f[k] = \left| \frac{k \cdot f_{\text{typ}} - F[k]}{k \cdot f_{\text{typ}} + \epsilon} \right| \quad (7)$$

126 where f_{typ} is the typical hourly fertilizer level the plant “expects” and ϵ is a
127 small constant preventing division by zero.

128 **Step 4: Cumulative divergence.** Apply EMA smoothing to track
129 sustained anomalies:

$$\Delta_f[k] = \beta_\Delta \Delta_f[k - 1] + (1 - \beta_\Delta) \delta_f[k] \quad (8)$$

130 where $\beta_\Delta = 0.95$ provides long memory.

131 **Step 5: Nutrient factor.** Convert divergence to a stress factor via
132 exponential decay with additional EMA smoothing:

$$\nu_f[k] = \beta_\nu \nu_f[k - 1] + (1 - \beta_\nu) \exp\{-\alpha \Delta_f[k]\} \quad (9)$$

133 where $\alpha = 3$ ensures $\nu \approx 0.05$ when $\Delta = 1$ (complete divergence from
134 expected levels), and $\beta_\nu = 0.05$.

135 The nutrient factor $\nu_f[k]$ equals 1 when fertilizer application perfectly
136 matches expected levels and decays toward 0 under sustained over- or under-
137 application. This captures the intuition that plants are resilient to brief
138 deviations but suffer cumulative damage from prolonged stress.

139 Figure ?? illustrates the FIR convolution and EMA smoothing operations
140 that constitute the metabolic transformation pipeline. The left panel shows
141 how the Gaussian FIR kernel spreads and delays input signals, while the
142 right panel demonstrates how EMA filtering with different β values tracks
143 cumulative divergence with varying memory lengths.

¹⁴⁴ 2.4. Effects of inputs on plant growth

¹⁴⁵ Different inputs affect different aspects of plant growth. Tables ?? and
¹⁴⁶ ?? summarize these relationships based on agronomic literature [? ? ?].

State variable	Irrigation on growth rate	Fertilizer on growth rate	Irrigation on capacity	Fertilizer on capacity
Plant height h	~	+	~	+
Leaf area A	~	+	+	+
Number of leaves N	~	~	~	~
Flower size c	~	~	+	~
Fruit biomass P	~	~	+	+

Table 1: Effects of irrigation and fertilizer on growth dynamics. “+” indicates positive effect, “~” indicates a negligible effect.

State variable	Temp. on growth rate	Temp. on capacity	Radiation on growth rate	Radiation on capacity
Plant height h	+	+	+	+
Leaf area A	+	+	+	+
Number of leaves N	~	+	~	+
Flower size c	-	-	-	-
Fruit biomass P	+	+	+	+

Table 2: Effects of temperature and solar radiation on growth dynamics. “+” indicates positive effect, “~” indicates a negligible effect, “-” indicates a negative effect. For flower size, excess heat and radiation reduce flower development, hence negative effects.

¹⁴⁷ 2.5. Growth dynamics

¹⁴⁸ Each state variable follows logistic growth with time-varying parameters
¹⁴⁹ modulated by nutrient factors. The general form is:

$$\frac{dx}{dt} = \hat{a}_x(t) \cdot x(t) \left(1 - \frac{x(t)}{\hat{k}_x(t)} \right) \quad (10)$$

150 where $\hat{a}_x(t)$ is the effective growth rate and $\hat{k}_x(t)$ is the effective carrying
 151 capacity, both functions of the nutrient factors.

152 The effective parameters are computed as geometric means of the relevant
 153 nutrient factors, reflecting multiplicative rather than additive effects. This
 154 choice is motivated by the observation that growth rates compound over
 155 time, making geometric averaging appropriate [?].

156 **Plant height** responds to fertilizer, temperature, and radiation:

$$\hat{a}_h(t) = a_h(\nu_f \nu_T \nu_R)^{1/3}, \quad \hat{k}_h(t) = k_h(\nu_f \nu_T \nu_R)^{1/3} \quad (11)$$

157 **Leaf area** additionally depends on water and is coupled to height:

$$\hat{a}_A(t) = a_A(\nu_f \nu_T \nu_R)^{1/3}, \quad \hat{k}_A(t) = k_A \left(\nu_w \nu_f \nu_T \nu_R \frac{\hat{k}_h}{k_h} \right)^{1/5} \quad (12)$$

158 **Number of leaves** depends only on temperature and radiation through
 159 the carrying capacity:

$$\hat{a}_N(t) = a_N, \quad \hat{k}_N(t) = k_N(\nu_T \nu_R)^{1/2} \quad (13)$$

160 **Flower size** (spikelet count) exhibits inverse dependence on temperature
 161 and radiation—excess heat and light reduce flowering:

$$\hat{a}_c(t) = a_c \left(\frac{1}{\nu_T} \frac{1}{\nu_R} \right)^{1/2}, \quad \hat{k}_c(t) = k_c \left(\nu_w \frac{1}{\nu_T} \frac{1}{\nu_R} \right)^{1/3} \quad (14)$$

162 **Fruit biomass** depends on all inputs and is coupled to vegetative growth:

$$\hat{a}_P(t) = a_P \left(\frac{1}{\nu_T} \frac{1}{\nu_R} \right)^{1/2}, \quad \hat{k}_P(t) = k_P \left(\nu_w \nu_f \nu_T \nu_R \frac{\hat{k}_h \hat{k}_A \hat{k}_c}{k_h k_A k_c} \right)^{1/7} \quad (15)$$

163 The coupling terms \hat{k}_h/k_h , \hat{k}_A/k_A , and \hat{k}_c/k_c encode physiological depen-
 164 dencies: taller plants with more leaf area can support larger fruit, while larger
 165 tassels (more spikelets) may compete with ear development.

166 2.6. Model parameters

167 The baseline growth rates and carrying capacities are crop-specific pa-
 168 rameters that can be estimated from field data or literature values. For corn,
 169 we use the values in Table ??, calibrated to match typical development time-
 170 lines where plants reach full vegetative size around 65–70 days after sowing
 171 and grain fill completes around 125 days [?].

State	Growth rate	Carrying capacity	Initial condition	Units
Height h	$a_h = 0.010 \text{ hr}^{-1}$	$k_h = 3.0$	$h_0 = 0.001$	m
Leaf area A	$a_A = 0.0105 \text{ hr}^{-1}$	$k_A = 0.65$	$A_0 = 0.001$	m^2
Leaves N	$a_N = 0.011 \text{ hr}^{-1}$	$k_N = 20$	$N_0 = 0.001$	count
Spikelets c	$a_c = 0.010 \text{ hr}^{-1}$	$k_c = 1000$	$c_0 = 0.001$	count
Fruit P	$a_P = 0.005 \text{ hr}^{-1}$	$k_P = 0.25$	$P_0 = 0.001$	kg

Table 3: Baseline model parameters for corn. Growth rates are per hour; initial conditions are set to k_x/K where $K \approx 2900$ is the season length in hours.

172 3. Simulation

173 The logistic ODE admits a closed-form solution, enabling exact time-
 174 stepping without numerical integration error. Given state $x(t)$ at time t , the
 175 state at $t + \Delta t$ is:

$$x(t + \Delta t) = \frac{\hat{k}_x(t)}{1 + \left(\frac{\hat{k}_x(t)}{x(t)} - 1 \right) \exp(-\hat{a}_x(t)\Delta t)} \quad (16)$$

176 where $\hat{a}_x(t)$ and $\hat{k}_x(t)$ are treated as constant over the time step. This closed-
 177 form approach is more accurate than forward Euler integration and avoids
 178 instability issues that can arise with explicit methods at larger time steps.

179 We simulate the growing season at hourly resolution ($\Delta t = 1$ hour),
 180 yielding approximately 2900 time steps for a typical corn season (late April
 181 to early October). At each step, we: (1) update the nutrient factors based on
 182 cumulative inputs and divergences, (2) compute effective growth rates and
 183 carrying capacities, and (3) advance each state variable using Equation ??.

184 4. Optimization via genetic algorithm

185 Given the nonlinear, delay-affected dynamics of the crop model, gradient-
 186 based optimization is challenging. The delayed effects of inputs create a
 187 non-convex landscape with potentially many local optima. We therefore
 188 employ a genetic algorithm (GA), a population-based metaheuristic inspired
 189 by natural selection that can effectively explore complex search spaces [?].

190 *4.1. Decision variables*

191 Each candidate solution encodes a complete irrigation and fertilization
 192 strategy as a four-dimensional vector:

$$\mathbf{u} = \begin{bmatrix} u_1 \\ u_2 \\ u_3 \\ u_4 \end{bmatrix} = \begin{bmatrix} \text{irrigation frequency (hours)} \\ \text{irrigation amount (inches)} \\ \text{fertilizer frequency (hours)} \\ \text{fertilizer amount (lbs)} \end{bmatrix} \quad (17)$$

193 The frequencies specify application intervals: $u_1 = 168$ means irrigate
 194 every 168 hours (weekly). The amounts specify the quantity applied at
 195 each event. This parameterization assumes regular, periodic application—a
 196 simplification that captures common agricultural practice while keeping the
 197 search space tractable.

198 *4.2. Objective function*

199 The objective is to maximize net revenue, defined as crop value minus
 200 input costs.

$$\text{Revenue}(\mathbf{u}) = \text{Crop Value} - \text{Input Costs} \quad (18)$$

201 The crop value depends on final plant state at harvest:

$$\text{Crop Value} = \omega_h h[K] + \omega_A A[K] + \omega_P P[K] \quad (19)$$

202 where K is the final time step and ω_h , ω_A , ω_P are economic weights (dollars
 203 per unit) for height, leaf area, and fruit biomass respectively.

204 The input costs accumulate over the season:

$$\text{Input Costs} = \omega_w \sum_{k=0}^K w[k] + \omega_f \sum_{k=0}^K f[k] \quad (20)$$

205 where ω_w and ω_f are costs per unit of irrigation and fertilizer.

206 For corn, the economic weights are derived from market prices and typical
 207 yields (Table ??). The fruit biomass weight dominates, reflecting that grain
 208 yield is the primary economic output.

Parameter	Value	Derivation
ω_w	\$2.00/inch	Typical irrigation cost
ω_f	\$0.61/lb	Weighted NPK cost
ω_h	\$35/m	Silage value proxy
ω_A	\$215/m ²	Silage value proxy
ω_P	\$4,450/kg	\$4/bushel × plant density

Table 4: Economic weights for the corn objective function. The fruit biomass weight accounts for approximately 28,350 plants per acre at \$0.157/kg.

209 *4.3. Algorithm description*

210 The GA maintains a population of M candidate solutions and iteratively
 211 improves them through selection, crossover, and mutation over G genera-
 212 tions. Algorithm ?? presents the complete procedure.

213 **Selection.** After each generation, population members are ranked by
 214 cost. The top P members survive as “parents” for the next generation. This
 215 selection ensures the best solutions are never lost.

216 **Crossover.** New “children” are created by blending two parent solutions.
 217 For each child, we randomly select two parents and compute a weighted
 218 average:

$$\mathbf{u}^{(\text{child})} = \phi \cdot \mathbf{u}^{(a)} + (1 - \phi) \cdot \mathbf{u}^{(b)} \quad (21)$$

219 where $\phi \sim \text{Uniform}(0, 1)$ under normal operation. This crossover can produce
 220 children anywhere along the line segment connecting the parents, enabling
 221 smooth exploration of the search space.

222 **Mutation and Diversity.** To maintain population diversity and escape
 223 local optima, the remaining $M - P - C$ population slots are filled with ran-
 224 domly generated solutions. Additionally, if the best cost stagnates (changes
 225 by less than 0.01) for 10 consecutive generations, we switch to aggressive
 226 crossover with $\phi \sim \text{Uniform}(-1, 2)$. This allows children to lie outside the
 227 convex hull of their parents, promoting exploration of new regions.

228 **Default Parameters.** We use $M = 128$ members, $P = 16$ parents,
 229 $C = 16$ children, and $G = 100$ generations. The large population relative
 230 to generations ensures diversity for exploration while preventing premature
 231 convergence.

232 5. Case study: corn in iowa

233 We demonstrate the framework using corn, the most widely planted crop
234 in the United States with over 90 million acres harvested annually [?].
235 The case study uses historical weather data from Fairfax, Iowa (41.76°N ,
236 91.87°W), a representative location in the Corn Belt (USDA climate zones
237 4b–5b).

238 5.1. Scenario configuration

239 The simulation covers a typical growing season from late April to early
240 October (approximately 2900 hours). Environmental inputs are:

- 241 • **Temperature and radiation:** Hourly data from NSRDB for Fairfax,
242 IA. Mean temperature is 22.8°C ; mean solar radiation is 580 W/m^2 .
- 243 • **Precipitation:** Daily data from NOAA, interpolated to hourly reso-
244 lution.
- 245 • **Typical nutrient expectations:** Based on agronomic recommenda-
246 tions [?], the model expects 28 inches of water and 355 lbs of NPK
247 fertilizer over the season ($w_{\text{typ}} \approx 0.01 \text{ in/hr}$, $f_{\text{typ}} \approx 0.12 \text{ lb/hr}$).

248 Table ?? summarizes expected corn development timelines used to cali-
249 brate model parameters.

State variable	Days to maturity	Hours to maturity	Typical final value
Plant height h	65–70	1560–1680	2.7–3.7 m
Leaf area A	55–65	1320–1560	0.6–0.7 m^2
Number of leaves N	65	1560	18–20
Spikelets c	65–70	1560–1680	~1000
Fruit biomass P	125	3000	0.15–0.36 kg

Table 5: Corn development timeline and typical final values from agronomic literature [?].

250 5.2. Baseline scenario: farmer best practices under drought

251 To establish a performance baseline, we first simulate crop growth under
252 a drought scenario (50% of typical precipitation) using conventional farmer
253 practices: weekly irrigation of 1 inch [?] and monthly fertilizer applications
254 of 90 lbs [?]. These values reflect standard agronomic recommendations for
255 corn in the Corn Belt region.

256 Figure ?? shows the environmental disturbances and control inputs over
257 the growing season. The reduced precipitation characteristic of a drought
258 year is clearly visible, along with the periodic irrigation and fertilizer appli-
259 cations.

260 Figure ?? shows the resulting plant state trajectories. Under drought
261 conditions with conventional management, the plant reaches the following
262 final values: height of 2.6 m (vs. 3.0 m capacity), leaf area of 0.57 m² (vs.
263 0.65 m²), and fruit biomass of 0.22 kg (vs. 0.25 kg). The net revenue under
264 this baseline scenario is \$859/acre.

265 The baseline scenario demonstrates how the model captures stress ef-
266 fects: despite regular irrigation, the mismatch between applied water and
267 the plant's metabolic expectations under drought conditions leads to sus-
268 tained nutrient factor depression and reduced growth potential. Detailed
269 visualizations of the applied vs. absorbed nutrients, cumulative values, and
270 nutrient factors are provided in the Supplementary Information.

271 5.3. Optimization configuration

272 The GA searches over the following bounds:

- 273 • Irrigation frequency: 100–700 hours (4–29 days between applications)
- 274 • Irrigation amount: 0.5–5.0 inches per application
- 275 • Fertilizer frequency: 700–2900 hours (29–121 days, i.e., 1–4 applications
276 per season)
- 277 • Fertilizer amount: 100–500 lbs per application

278 These bounds reflect practical constraints: irrigation systems have mini-
279 mium application rates, and fertilizer is typically applied in a small number of
280 large doses rather than continuously. The optimization was performed under
281 the same environmental conditions: a drought scenario with 50% of typical
282 precipitation.

283 5.4. Optimization results

284 To assess robustness of the optimization, we executed 10 independent
285 GA runs with different random seeds. Figure ?? shows the convergence of
286 all 10 runs, with each curve representing the best revenue achieved at each
287 generation. All runs converge to similar final values (within 3% of each other),
288 demonstrating that the GA reliably finds near-optimal solutions despite the
289 stochastic nature of the search.

290 The optimal strategy identified by the GA is summarized in Table ??.
291 Notably, the algorithm discovers a strategy with less frequent but larger
292 irrigation events and infrequent fertilizer applications—a pattern that mini-
293 mizes cumulative divergence from expected nutrient levels given the model’s
294 delayed absorption dynamics.

Parameter	Optimal Value	Interpretation
Irrigation frequency	1237 hours	Every \sim 7 weeks
Irrigation amount	5 inches	Per application
Fertilizer frequency	803 hours	Every 33 days
Fertilizer amount	77 lbs	Per application

Table 6: Optimal irrigation and fertilization strategy identified by the GA.

295 Figure ?? shows the plant state trajectories for the best member in each
296 of the 10 GA runs. All optimized strategies achieve substantially higher final
297 values than the baseline farmer practices: fruit biomass ranges from 0.168–
298 0.225 kg (vs. 0.22 kg baseline), heights reach 2.41–2.88 m (vs. 2.6 m), leaf
299 areas reach 0.44–0.56 m² (vs. 0.57 m²), and revenues reach 778–999 \$/acre
300 (vs. \$859/acre baseline). The consistency across runs further confirms the
301 robustness of the optimization, and while the farmer best practice yields
302 higher revenue than one GA run (run 2), in aggregate, the GA optimization
303 meaningfully improved upon the baseline.

304 Table ?? provides an economic comparison between the baseline farmer
 305 practices and the GA-optimized strategies. The best GA strategy achieves
 306 \$999/acre net revenue compared to \$859/acre for the baseline—a 16% im-
 307 provement. Even the worst members in each GA run’s final population out-
 308 perform the baseline, providing a sanity check that random strategies are not
 309 viable (see Supplementary Information).

Metric	GA-Optimized	Baseline
Final fruit biomass	0.22 kg	0.22 kg
Final height	2.8 m	2.6 m
Final leaf area	0.60 m ²	0.57 m ²
Total irrigation	15 inches	18 inches
Total fertilizer	307 lbs	450 lbs
Crop value	\$1218	\$1171
Input costs	\$219	\$312
Revenue	\$999	\$859

Table 7: Economic comparison of GA-optimized versus baseline farmer strategies. The optimized strategy achieves 16% higher net revenue through both increased crop value and dramatically reduced irrigation costs.

310 6. Discussion

311 6.1. Interpretation of results

312 The GA-optimized strategy differs from conventional wisdom in several
 313 notable ways. The algorithm discovers that less frequent but larger irrigation
 314 events, combined with reduced total fertilizer input, can outperform conven-
 315 tional uniform application schedules. This counterintuitive result emerges
 316 from the model’s delayed absorption dynamics: under drought conditions,
 317 the plant’s metabolic expectations are calibrated to typical water availabil-
 318 ity. The GA discovers that strategically-timed resource inputs better main-
 319 tain alignment with metabolic expectations than aggressive compensation
 320 for drought through frequent, uniform applications.

321 The consistency across 10 independent GA runs provides confidence that
 322 the optimization reliably identifies high-performing regions of the strategy
 323 space. While individual runs converge to somewhat different local optima
 324 (with revenues ranging from \$778 to \$983 per acre), 9 of 10 runs outperform

325 the baseline farmer practices, demonstrating the robustness of the optimization
326 approach. The sanity check showing that even the worst members in
327 each final population generally outperform baseline practices confirms that
328 the GA successfully eliminates poor candidates.

329 The 16% revenue improvement (\$999 vs. \$859 per acre) demonstrates sub-
330 stantial potential value from model-based optimization. This improvement
331 comes from two sources: (1) increased crop value due to better-aligned nu-
332 trient delivery, and (2) reduced input costs. The result suggests that conven-
333 tional wisdom about drought response—applying more water to compensate—
334 may be suboptimal when plant physiology involves delayed, cumulative-effect
335 dynamics.

336 6.2. Parameter estimation in practice

337 The framework requires crop-specific parameters: growth rates, carrying
338 capacities, metabolic timescales, and typical nutrient expectations. Several
339 approaches could estimate these from data:

- 340 • **Growth curves:** Time-series imagery from field cameras or drones,
341 processed with computer vision, could provide height and leaf area
342 trajectories for fitting a_x and k_x parameters.
- 343 • **Metabolic timescales:** The temporal spreads σ could be estimated
344 from controlled experiments varying input timing, or inferred from
345 physiological literature on nutrient uptake rates.
- 346 • **Typical expectations:** Regional agronomic recommendations pro-
347 vide baseline values for w_{typ} , f_{typ} , T_{typ} , and R_{typ} .

348 Physics-informed neural networks (PINNs) could jointly fit model param-
349 eters and approximate unknown functional forms in the dynamics, potentially
350 relaxing some of the structural assumptions in Section ??.

351 6.3. Limitations and extensions

352 Several model limitations suggest directions for future work:

353 **Growth model.** The logistic equation assumes symmetric growth around
354 the inflection point. Richards growth [?] generalizes this with a shape pa-
355 rameter ν :

$$\frac{dx}{dt} = a_x x \left[1 - \left(\frac{x}{k_x} \right)^\nu \right] \quad (22)$$

356 where $\nu > 1$ produces steeper early growth (common in vegetative stages)
357 and $\nu < 1$ produces steeper late growth.

358 **Absorption kernels.** Gaussian kernels are symmetric, but physiological
359 absorption often exhibits fast activation followed by slow decay. Log-normal
360 or Gamma kernels could better capture this asymmetry.

361 **Saturation.** The current model does not explicitly limit nutrient uptake—
362 all applied inputs eventually affect the plant. In reality, excess application
363 may be lost to runoff or leaching. Saturating nonlinearities in the absorption
364 pathway would provide a more realistic response to over-application.

365 **Spatial heterogeneity.** The model treats a single representative plant.
366 Field-scale optimization would need to account for spatial variation in soil
367 properties, microclimate, and plant density.

368 **Stochastic weather.** The case study uses historical weather data. Robust
369 optimization under weather uncertainty, or adaptive strategies that respond
370 to observed conditions, could improve real-world performance.

371 7. Conclusion

372 This paper presented a coupled ODE model for crop growth that captures
373 delayed nutrient absorption via FIR convolution and cumulative stress
374 effects via EMA filtering. The model’s time-varying growth rates and carrying
375 capacities encode the intuition that plant development depends not just
376 on current conditions but on the history of resource availability relative to
377 physiological expectations.

378 Applied to corn optimization in Iowa under drought conditions, a genetic
379 algorithm discovered irrigation and fertilizer strategies that achieve
380 16% higher net revenue than conventional farmer practices (\$999 vs. \$859
381 per acre). This improvement emerges from the model’s delayed absorption
382 dynamics: strategic timing of inputs that aligns with metabolic expectations
383 outperforms uniform application schedules. The consistency across 10 independent
384 optimization runs, with 9 of 10 outperforming the baseline, confirms
385 the robustness of these findings.

386 The framework is generalizable to other crops through re-parameterization
387 and offers a computationally tractable approach to input optimization. Future
388 work will extend the model to handle weather uncertainty, incorporate
389 spatial heterogeneity, and validate predictions against field trial data.

390 **8. Supplementary information**

391 This supplementary section provides additional visualizations of the base-
392 line scenario (farmer best practices under drought) and the GA optimization
393 results.

394 *S1. Detailed baseline scenario analysis*

395 Figure ?? shows the applied versus absorbed nutrients under the baseline
396 scenario. The delayed absorption via FIR convolution is clearly visible: the
397 absorbed signals (smoothed curves) lag behind the applied inputs and exhibit
398 the characteristic spreading effect of the Gaussian kernels.

399 Figure ?? shows the cumulative absorbed nutrients compared to expected
400 (typical) levels. Under drought conditions, actual water absorption falls pro-
401 gressively below expectations, while fertilizer, temperature, and radiation
402 track more closely to typical values.

403 Figure ?? shows the instantaneous divergence from expected cumulative
404 levels. These divergences, after EMA smoothing, determine the nutrient
405 factors that modulate plant growth.

406 Figure ?? shows the resulting nutrient factors. The water factor ν_w de-
407 clines throughout the season as drought stress accumulates, reaching approx-
408 imately 0.6 by harvest. This reduced water factor is the primary driver of
409 the suboptimal crop growth observed in the baseline scenario.

410 *S2. GA optimization: worst-case analysis*

411 As a sanity check, Figure ?? shows the plant state trajectories for the
412 *worst* member in each GA run’s final population. Even these subopti-
413 mal strategies—the least fit survivors after 100 generations of evolution—
414 outperform the baseline farmer practices. This confirms that: (1) the GA
415 successfully eliminates poor strategies, and (2) random or arbitrary irri-
416 gation/fertilization schedules cannot match even the worst optimized ap-
417 proaches.

418 **9. Acknowledgements**

419 This work has been partially supported by the UC Berkeley College of
420 Engineering and the USDA AI Institute for Next Generation Food Systems
421 (AIFS), USDA award number 2020-67021-32855.

422 **Declarations**

423 **Competing Interests** The authors declare that they have no known com-
424 peting financial interests or personal relationships that could have appeared
425 to influence the work reported in this paper.

426 **Code availability** The source code used for this study is archived on Zen-
427 odo at <https://doi.org/10.5281/zenodo.18204023>.

429 **Declaration of generative AI and AI-assisted technologies in the
430 manuscript preparation process** During the preparation of this work the
431 authors used ChatGPT and Claude Code in order to generate some portions
432 of the code base, though no underlying theory, and refine the original drafts of
433 the paper. After using this tool/service, the authors reviewed and edited the
434 content as needed and take full responsibility for the content of the published
435 article.

437 **References**

- 438 [1] Economic Research Service, Farm income and wealth statistics, US
439 Department of Agriculture (2024).
440 URL [https://www.ers.usda.gov/data-products/
441 farm-income-and-wealth-statistics/](https://www.ers.usda.gov/data-products/farm-income-and-wealth-statistics/)
- 442 [2] T. I. Zohdi, A machine-learning enabled digital-twin framework for
443 next generation precision agriculture and forestry, Computer Meth-
444 ods in Applied Mechanics and Engineering 428 (2024) 117250. doi:
445 [10.1016/j.cma.2024.117250](https://doi.org/10.1016/j.cma.2024.117250).
- 446 [3] E. Mengi, C. J. Becker, M. Sedky, S. Yu, T. I. Zohdi, A digital-twin
447 and rapid optimization framework for optical design of indoor farming
448 systems, Computational Mechanics 72 (2023) 953–970. doi:[10.1007/s00466-023-02421-9](https://doi.org/10.1007/s00466-023-02421-9).

- 450 [4] P. Goodrich, O. Betancourt, A. Arias, T. I. Zohdi, Placement and drone
451 flight path mapping of agricultural soil sensors using machine learning,
452 Computers and Electronics in Agriculture 198 (2022) 107591. doi:10.
453 1016/j.compag.2022.107591.
- 454 [5] I. Tagkopoulos, S. F. Brown, X. Liu, Q. Zhao, T. I. Zohdi, J. M. Earles,
455 N. Nitin, D. E. Runcie, D. G. Lemay, A. D. Smith, P. C. Ronald, H. Feng,
456 G. D. Youtsey, Special report: AI institute for next generation food
457 systems (AIFS), Computers and Electronics in Agriculture 196 (2022)
458 106819. doi:10.1016/j.compag.2022.106819.
- 459 [6] P.-F. Verhulst, Notice sur la loi que la population suit dans son accroissement,
460 Correspondance mathématique et physique 10 (1838) 113–126.
461 doi:10.1007/BF02309004.
- 462 [7] J. W. Jones, G. Hoogenboom, C. H. Porter, K. J. Boote, W. D. Batchelor,
463 L. Hunt, P. W. Wilkens, U. Singh, A. J. Gijsman, J. T. Ritchie, The
464 dssat cropping system model, European Journal of Agronomy 18 (3-4)
465 (2003) 235–265. doi:10.1016/S1161-0301(02)00107-7.
- 466 [8] D. P. Holzworth, N. I. Huth, P. G. deVoil, E. J. Zurcher, N. I. Herrmann,
467 G. McLean, K. Chenu, E. J. van Oosterom, V. Snow, C. Murphy,
468 et al., Apsim—evolution towards a new generation of agricultural systems
469 simulation, Environmental Modelling & Software 62 (2014) 327–350.
470 doi:10.1016/j.envsoft.2014.07.009.
- 471 [9] C. Van Diepen, J. Wolf, H. Van Keulen, C. Rappoldt, Wofost: a simu-
472 lation model of crop production, Soil Use and Management 5 (1) (1989)
473 16–24. doi:10.1111/j.1475-2743.1989.tb00755.x.
- 474 [10] R. Gebbers, V. I. Adamchuk, Precision agriculture and food security,
475 Science 327 (5967) (2010) 828–831. doi:10.1126/science.1183899.
- 476 [11] A. Singh, An overview of the optimization modelling applications, Jour-
477 nal of Hydrology 466–467 (2012) 167–182. doi:10.1016/j.jhydrol.
478 2012.08.004.
- 479 [12] J. E. Epperson, J. E. Hook, Y. R. Mustafa, Dynamic program-
480 ming for improving irrigation scheduling strategies of maize,
481 Agricultural Systems 42 (1) (1993) 85–101, applications of

- 482 Dynamic Optimization Techniques to Agricultural Problems.
483 doi:[https://doi.org/10.1016/0308-521X\(93\)90070-I](https://doi.org/10.1016/0308-521X(93)90070-I).
484 URL <https://www.sciencedirect.com/science/article/pii/0308521X9390070I>
- 486 [13] W. Ding, C. Lin, Application of genetic algorithms to agriculture: a
487 review, Computers and Electronics in Agriculture 175 (2020) 105524.
488 doi:[10.1016/j.compag.2020.105524](https://doi.org/10.1016/j.compag.2020.105524).
- 489 [14] D. E. Goldberg, Genetic Algorithms in Search, Optimization, and Ma-
490 chine Learning, Addison-Wesley, Reading, MA, 1989.
- 491 [15] R. Wardlaw, K. Bhaktikul, Application of genetic algorithms for irriga-
492 tion water scheduling, Irrigation and Drainage 53 (4) (2004) 397–414.
493 doi:[10.1002/ird.121](https://doi.org/10.1002/ird.121).
- 494 [16] Z. Yu, W. Fu, Optimization of nitrogen fertilization strategies for drip
495 irrigation of cotton in large fields by dssat combined with a genetic
496 algorithm, Applied Sciences 15 (7) (2025) 3580.
- 497 [17] M. Sengupta, Y. Xie, A. Lopez, A. Habte, G. MacLaurin, J. Shelby, The
498 national solar radiation data base (nsrdb), Renewable and Sustainable
499 Energy Reviews 89 (2018) 51–60. doi:[10.1016/j.rser.2018.03.003](https://doi.org/10.1016/j.rser.2018.03.003).
- 500 [18] National Oceanic and Atmospheric Administration, Climate data online
501 (2024).
502 URL <https://www.ncdc.noaa.gov/cdo-web/>
- 503 [19] J. E. Sawyer, E. D. Nafziger, G. W. Randall, L. G. Bundy, G. W.
504 Rehm, B. C. Joern, Nitrogen management for corn production, Iowa
505 State University Extension Publication PM 1714 (2006).
- 506 [20] J. O. Payero, D. D. Tarkalson, S. Irmak, D. R. Davison, J. L. Petersen,
507 Effect of irrigation amounts applied with subsurface drip irrigation on
508 corn evapotranspiration, yield, water use efficiency, and dry matter pro-
509 duction in a semiarid climate, Agricultural Water Management 95 (8)
510 (2008) 895–908. doi:[10.1016/j.agwat.2008.02.015](https://doi.org/10.1016/j.agwat.2008.02.015).
- 511 [21] B. Sánchez, A. Rasmussen, J. R. Porter, Temperatures and the growth
512 and development of maize and rice: a review, Global Change Biology
513 20 (2) (2014) 408–417. doi:[10.1111/gcb.12389](https://doi.org/10.1111/gcb.12389).

- 514 [22] R. C. Lewontin, D. Cohen, On population growth in a randomly varying
515 environment, *Proceedings of the National Academy of Sciences* 62 (4)
516 (1969) 1056–1060. doi:10.1073/pnas.62.4.1056.
- 517 [23] L. J. Abendroth, R. W. Elmore, M. J. Boyer, S. K. Marlay, In corn
518 growth and development, Iowa State University Extension Publication
519 PMR 1009 (2011).
- 520 [24] US Department of Agriculture, 2023 acreage data as of august 9, 2023
521 (2023).
- 522 [25] J. Sawyer, E. Nafziger, G. Randall, L. Bundy, G. Rehm, B. Joern, Con-
523 cepts and rational for regional nitrogen rate guidelines for corn, Univer-
524 sity Extension Iowa State University Ames (2006).
- 525 [26] F. Schierbaum, Book reviews: Corn: Chemistry and technology, 2nd
526 edition. by pamela j. white and lawrence a. johnson (editors), Starch-
527 starke - STARCH 56 (2004) 263–264. doi:10.1002/star.200490027.
- 528 [27] W. L. Kranz, S. Irmak, S. J. van Donk, C. D. Yonts, D. L. Martin, Irri-
529 gation management for corn, Tech. Rep. G1850, University of Nebraska–
530 Lincoln Extension (2008).
531 URL <https://extensionpubs.unl.edu/publication/g1850/>
- 532 [28] B. Davies, J. A. Coulter, P. H. Pagliari, Timing and rate of nitrogen
533 fertilization influence maize yield and nitrogen use efficiency, *PLOS ONE*
534 15 (5) (2020) e0233674. doi:10.1371/journal.pone.0233674.
- 535 [29] F. J. Richards, A flexible growth function for empirical use, *Journal of*
536 *Experimental Botany* 10 (2) (1959) 290–301. doi:10.1093/jxb/10.2.
537 290.

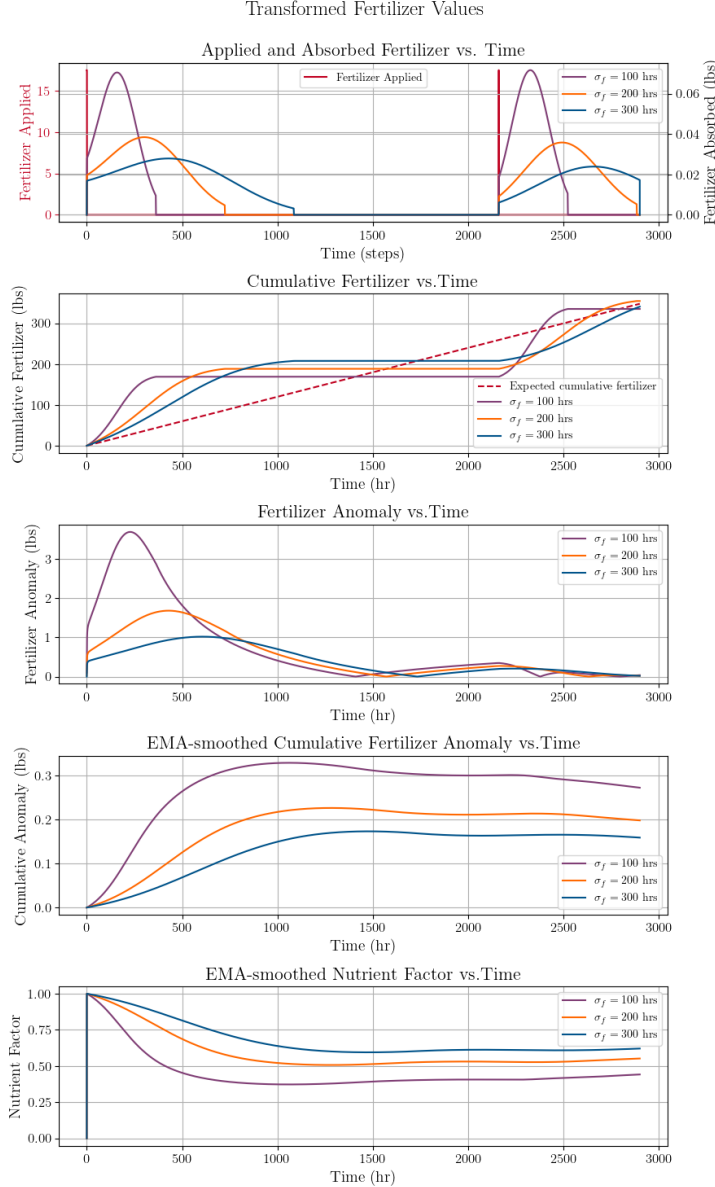


Figure 1: Illustration of the metabolic transformation pipeline. Panel 1: Gaussian FIR kernels with different temporal spreads σ demonstrate how water ($\sigma_w = 30$ hr) is absorbed more rapidly than fertilizer ($\sigma_f = 300$ hr). Panel 4: EMA filters with different memory parameters β show how cumulative divergence tracking responds to sustained anomalies, with larger β providing longer memory of past stress events.

Algorithm 1 Genetic Algorithm for Input Optimization

- 1: **Input:** Population size M , parents P , children C , generations G , bounds $[\mathbf{u}_{\min}, \mathbf{u}_{\max}]$
- 2: **Output:** Best solution \mathbf{u}^*
- 3:
- 4: Initialize population $\{\mathbf{u}^{(1)}, \dots, \mathbf{u}^{(M)}\}$ uniformly in bounds
- 5: Evaluate Cost($\mathbf{u}^{(i)}$) for all i via full-season simulation
- 6: Sort population by cost (ascending)
- 7: stagnation $\leftarrow 0$
- 8:
- 9: **for** $g = 1$ to G **do**
- 10: **Selection:** Keep top P members as parents
- 11:
- 12: **Crossover:** Generate C children
- 13: **for** $j = 1$ to C **do**
- 14: Select parents $\mathbf{u}^{(a)}, \mathbf{u}^{(b)}$ randomly from top P
- 15: **if** stagnation < 10 **then**
- 16: $\phi \sim \text{Uniform}(0, 1)$
- 17: **else**
- 18: $\phi \sim \text{Uniform}(-1, 2)$ ▷ Aggressive exploration
- 19: **end if**
- 20: $\mathbf{u}^{(\text{child})} \leftarrow \phi \cdot \mathbf{u}^{(a)} + (1 - \phi) \cdot \mathbf{u}^{(b)}$
- 21: Clip to bounds
- 22: **end for**
- 23:
- 24: **Fill remaining:** Generate $M - P - C$ random members
- 25: Evaluate costs for new members
- 26: Sort population by cost
- 27:
- 28: **Stagnation check:**
- 29: **if** $|\text{Cost}^{(g)} - \text{Cost}^{(g-1)}| < 0.01$ **then**
- 30: stagnation \leftarrow stagnation + 1
- 31: **else**
- 32: stagnation $\leftarrow 0$
- 33: **end if**
- 34: **end for**
- 35:
- 36: **return** $\mathbf{u}^{(1)}$ (best member)

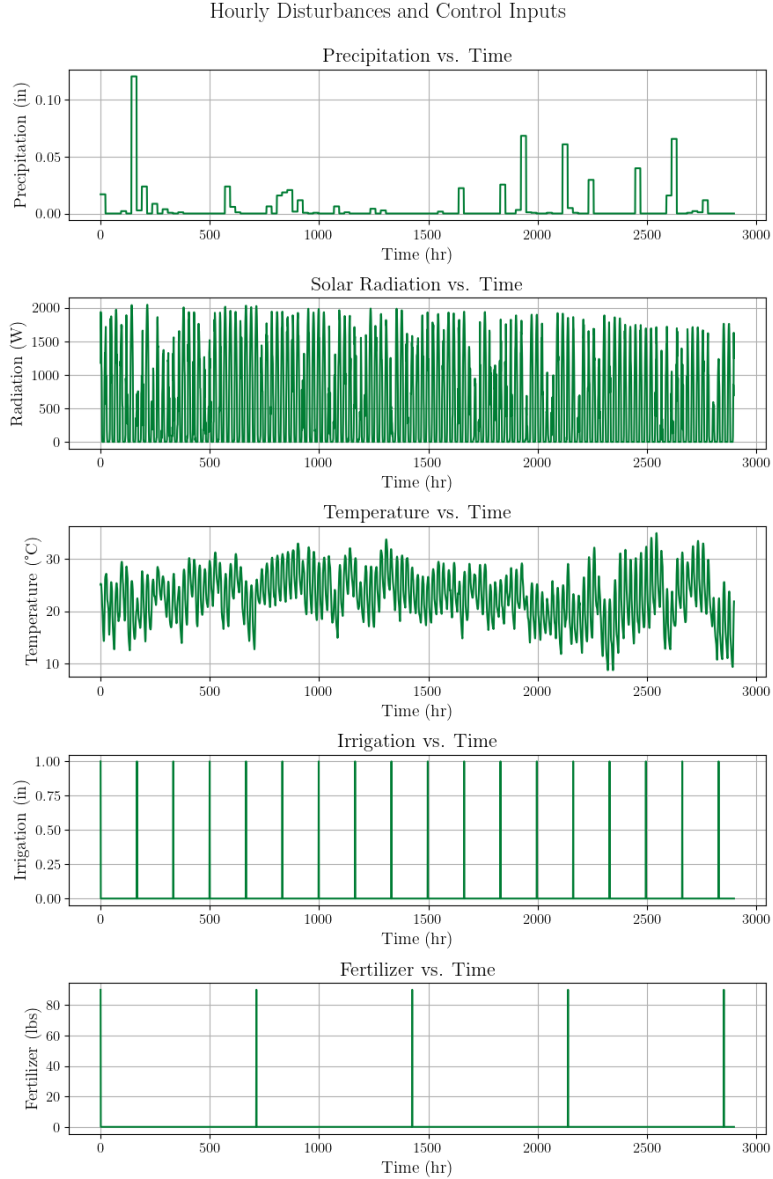


Figure 2: Environmental disturbances and control inputs for the baseline scenario. Top three panels show hourly precipitation (reduced to 50% of normal), solar radiation, and temperature from historical Iowa data. Bottom two panels show the farmer's irrigation (weekly, 1 inch) and fertilizer (monthly, 90 lbs) application strategy.

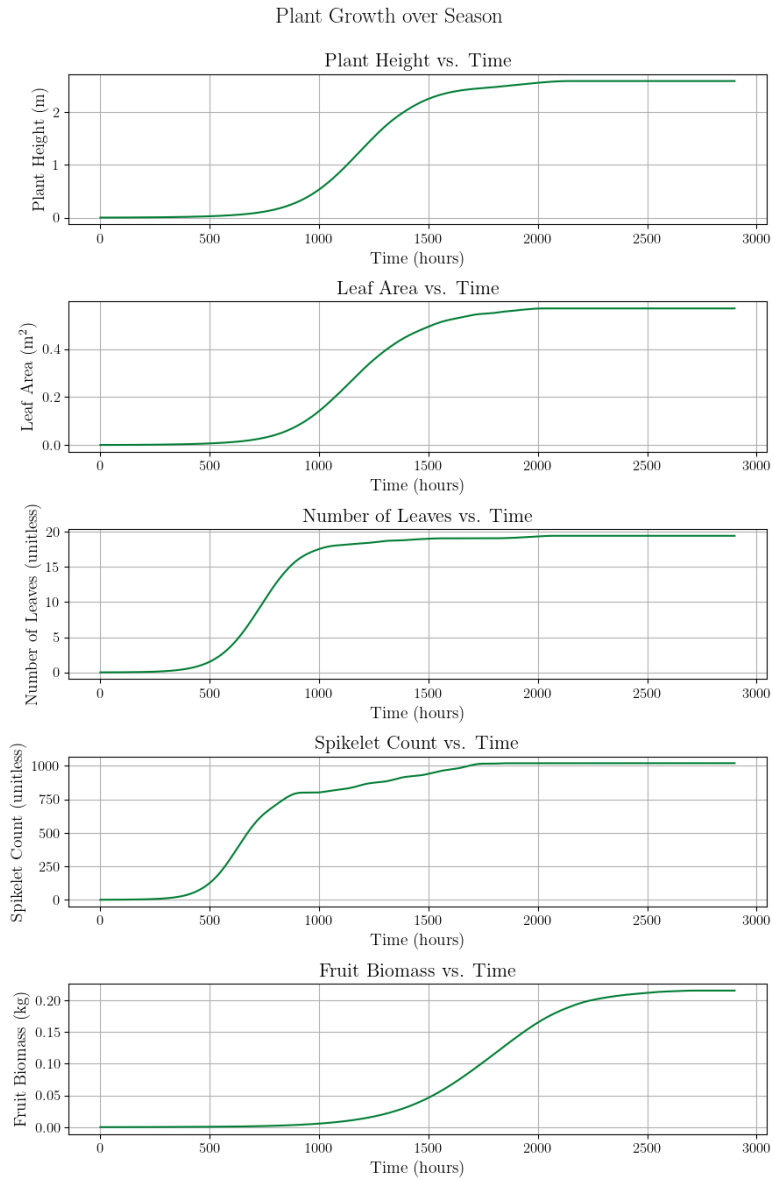


Figure 3: Plant state variable trajectories under the baseline scenario (farmer best practices during drought). All state variables reach suboptimal final values due to cumulative water stress. This strategy yields \$859/acre in revenue.

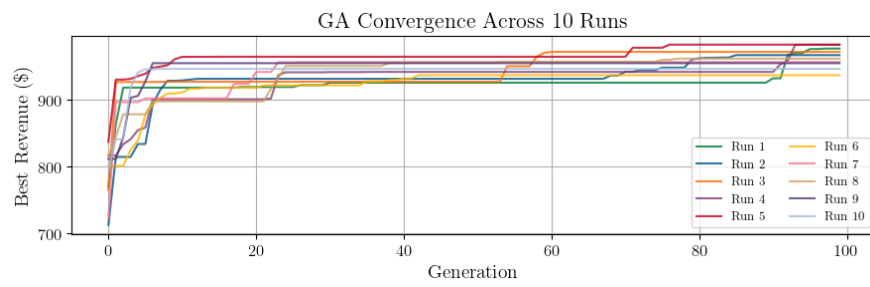


Figure 4: GA convergence across 10 independent runs. Each curve shows the best revenue at each generation. All runs exhibit rapid improvement in early generations followed by convergence to near-optimal solutions. The consistency across runs demonstrates algorithm robustness.

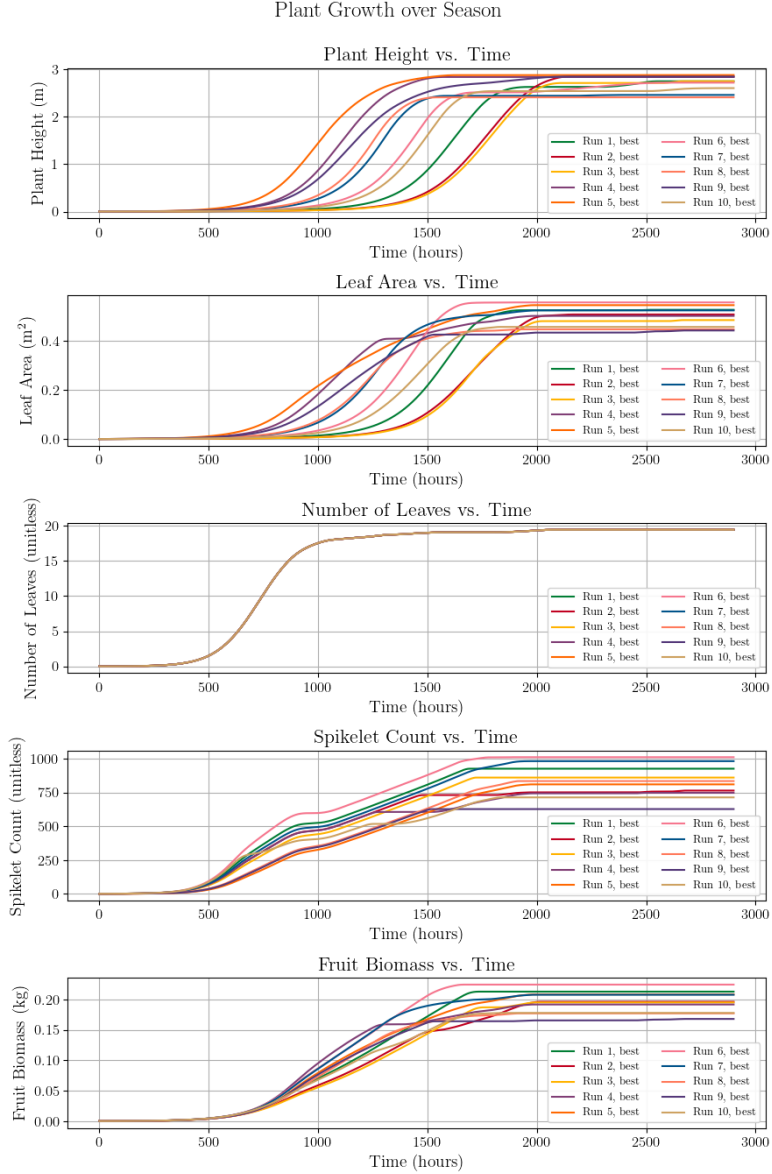


Figure 5: Plant state variable trajectories for the best member from each of the 10 independent GA runs. All optimized strategies achieve similar, near-optimal growth trajectories, and 9 of 10 runs substantially outperform the baseline farmer practices (Figure ??). The tight clustering of trajectories demonstrates that different GA runs converge to similar optimal strategies.

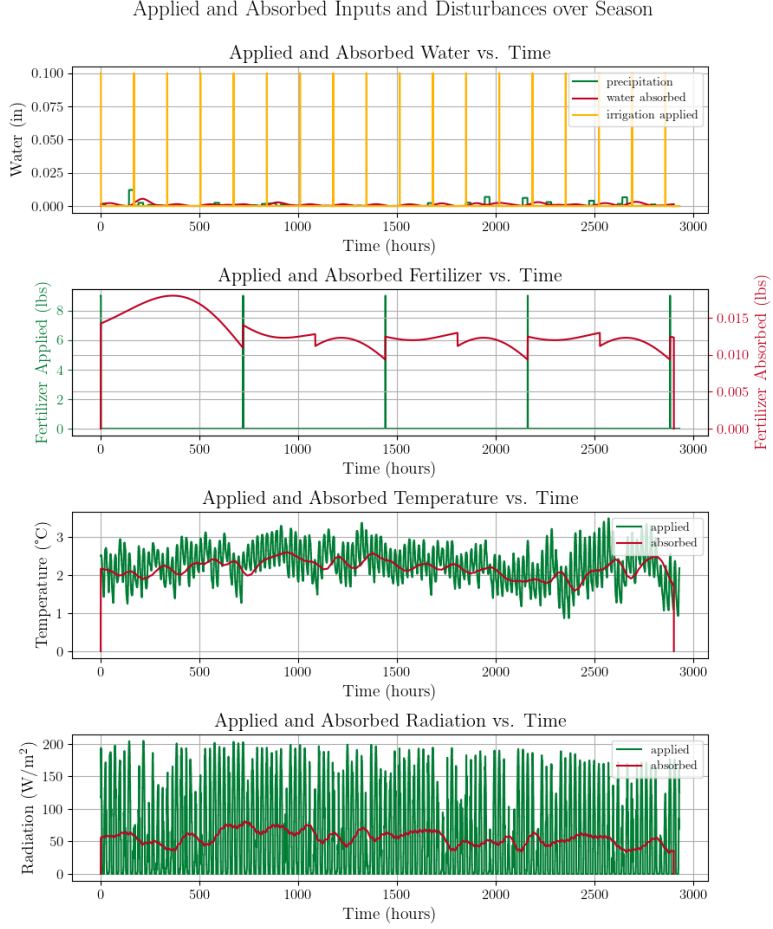


Figure 6: Applied versus absorbed nutrients under the baseline farmer strategy. The delayed absorption dynamics are evident in the lag between applied inputs and the smoothed absorbed signals. Water absorption ($\sigma_w = 30$ hr) responds more quickly than fertilizer absorption ($\sigma_f = 300$ hr).

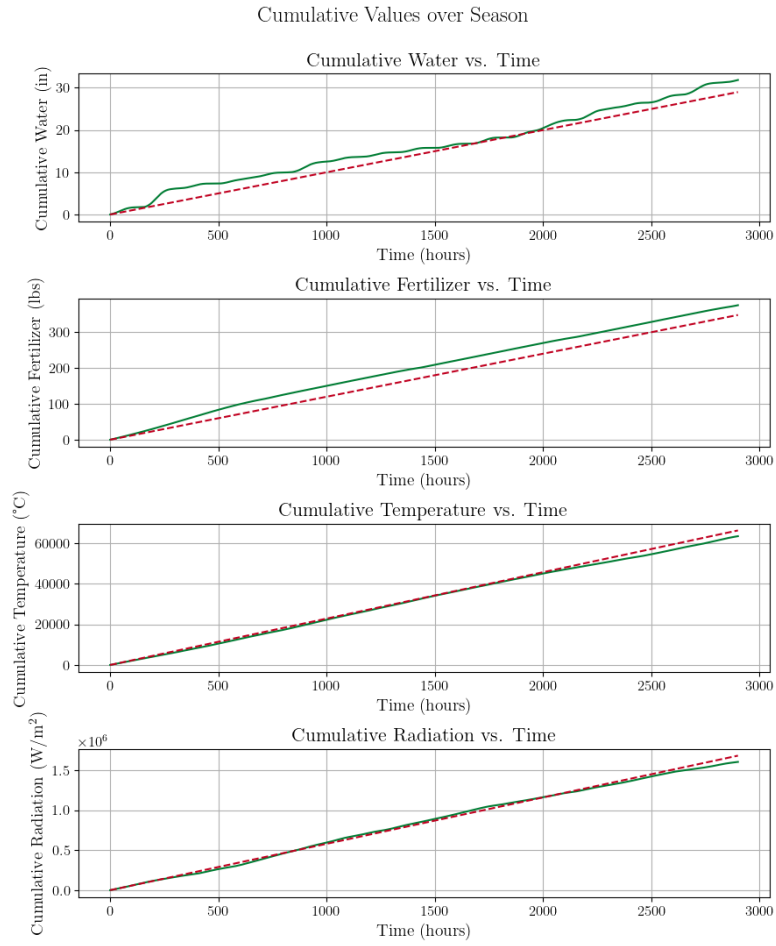


Figure 7: Cumulative absorbed nutrients (solid) versus expected levels (dashed red). The growing gap between actual and expected water absorption reflects the drought stress accumulating over the season. Fertilizer applications maintain closer alignment with expectations.

Differences between Actual and Typical Cumulative Values

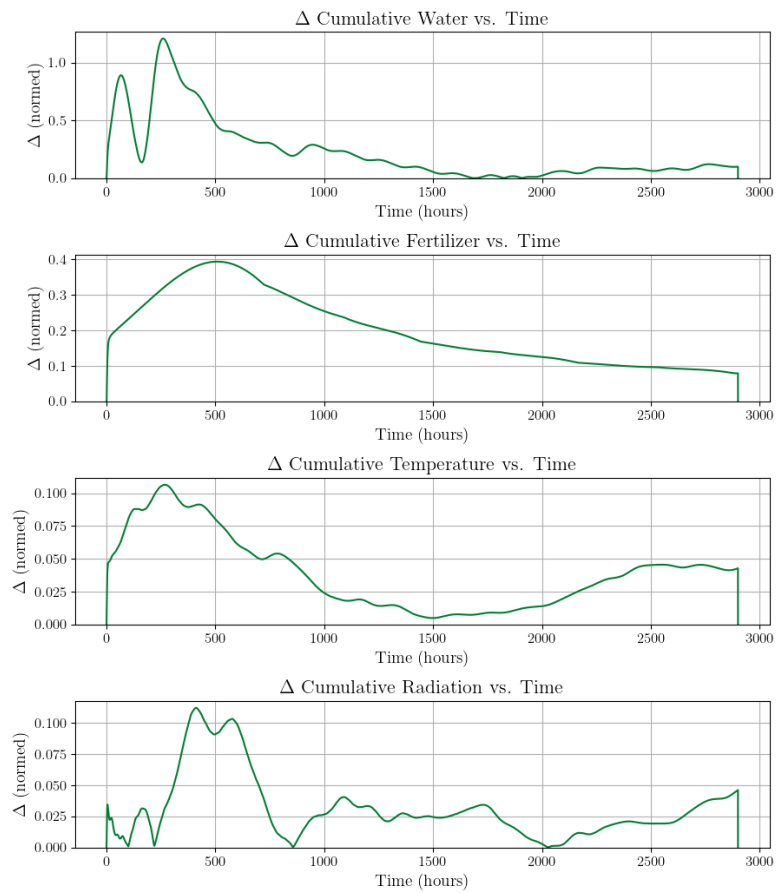


Figure 8: Instantaneous divergence from expected cumulative nutrient levels. Higher divergence indicates greater stress. The water divergence grows throughout the season due to cumulative drought effects.

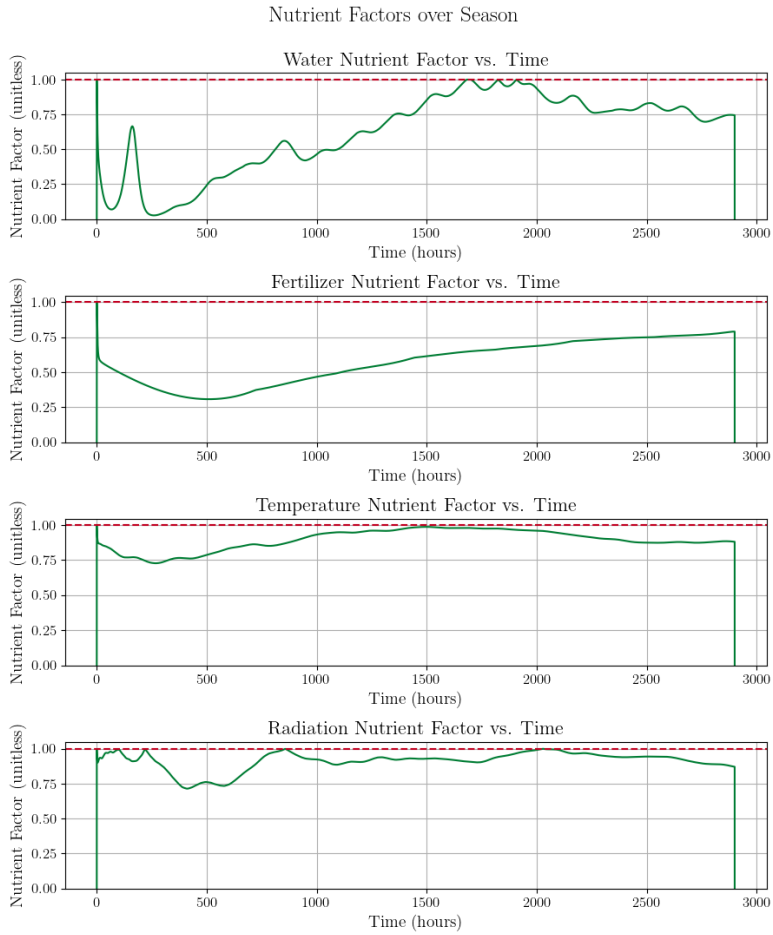


Figure 9: Nutrient factor evolution under the baseline scenario. The water factor ν_w declines due to cumulative drought stress, while fertilizer, temperature, and radiation factors remain closer to 1.0 (no stress). The declining ν_w reduces effective growth rates and carrying capacities throughout the season.

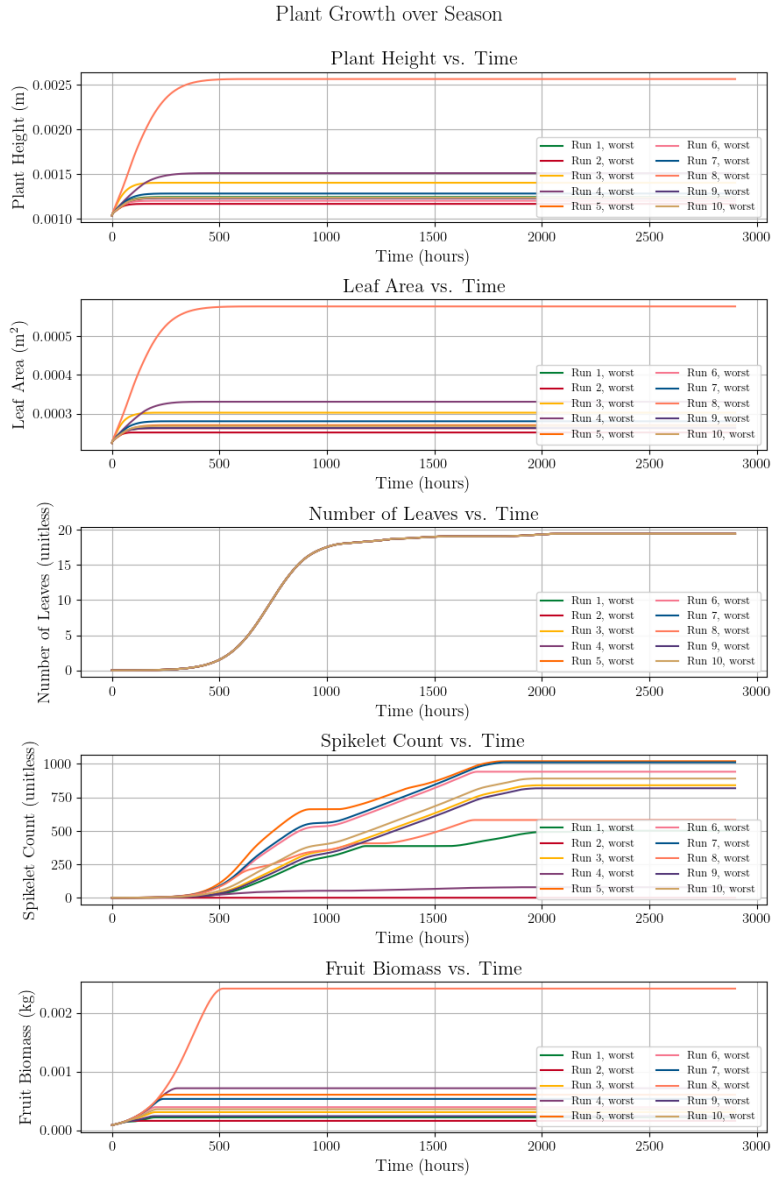


Figure 10: Plant state variable trajectories for the worst member from each GA run’s final population. Even these suboptimal strategies outperform baseline farmer practices (compare to Figure ??), demonstrating that the GA successfully identifies the high-performing region of the strategy space and that random strategies are not competitive.